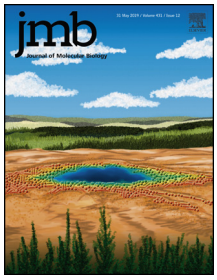

# Potential Regulatory Role of Competitive Encounter Complexes in Paralogous Phosphotransferase Systems

**Madeleine Strickland [1], Seyit Kale [1], Marie-Paule Strub [1], Charles D. Schwieters [2], Jian Liu [1], Alan Peterkofsky [3 †] and Nico Tjandra [1]**

*1 - **Biochemistry and Biophysics Center,** National Heart, Lung, and Blood Institute, National Institutes of Health, Bethesda, MD 20892, USA*
*2 - **Office of Intramural Research,** Center for Information Technology, National Institutes of Health, Bethesda, MD 20892, USA*
*3 - **Cell Biology and Physiology Center,** National Heart, Lung, and Blood Institute, National Institutes of Health, Bethesda, MD 20892, USA*

***Correspondence to Alan Peterkofsky and Nico Tjandra:** Building 50, Room 3503, NHLBI, NIH, Bethesda, MD 20892, USA. peterkoa@nhlbi.nih.gov, tjandran@nhlbi.nih.gov*
https://doi.org/10.1016/j.jmb.2019.04.040
***Edited by Sheena Radford***

## Abstract

There are two paralogous *Escherichia coli* phosphotransferase systems, one for sugar import ($PTS^{sugar}$) and one for nitrogen regulation ($PTS^{Ntr}$), that utilize proteins enzyme $I^{sugar}$ ($EI^{sugar}$) and HPr, and enzyme $I^{Ntr}$ ($EI^{Ntr}$) and NPr, respectively. The enzyme I proteins have similar folds, as do their substrates HPr and NPr, yet they show strict specificity for their cognate partner both in stereospecific protein–protein complex formation and in reversible phosphotransfer. Here, we investigate the mechanism of specific $EI^{Ntr}$:NPr complex formation by the study of transient encounter complexes. NMR paramagnetic relaxation enhancement experiments demonstrated transient encounter complexes of $EI^{Ntr}$ not only with the expected partner, NPr, but also with the unexpected partner, HPr. HPr occupies transient sites on $EI^{Ntr}$ but is unable to complete stereospecific complex formation. By occupying the non-productive transient sites, HPr promotes NPr transient interaction to productive sites closer to the stereospecific binding site and actually enhances specific complex formation between NPr and $EI^{Ntr}$. The cellular level of HPr is approximately 150 times higher than that of NPr. Thus, our finding suggests a potential mechanism for cross-regulation of enzyme activity through formation of competitive encounter complexes.



## Introduction

In bacteria, the phosphoenolpyruvate-dependent carbohydrate phosphotransferase system ($PTS^{sugar}$) drives the uptake of carbohydrates across the inner membrane, as well as their subsequent phosphorylation [1,2] (for review, see Ref. [3]). The $PTS^{sugar}$ comprises a five-step cascade initiated by phosphoenolpyruvate, a glycolytic intermediate, and involves three proteins, namely, enzyme I (EI), the phosphocarrier protein (HPr), and enzyme II (EII). While EI and HPr are generic phosphoryl accepting transferases shared by various transport PTSs, EII is a carbohydrate-specific permease [4]. EIIs contain three subdomains—the cytosolic phosphoryl-accepting proteins EIIA and EIIB, and the carbohydrate binding transmembrane EIIC, which is responsible for ligand selectivity and unilateral translocation [5]. These components are either arranged as a single protein unit or as interacting chains, all with various but important quaternary arrangements and shared interfaces [6–9]. PTS proteins, through their extent of phosphorylation or the nature of the carbohydrate, are also associated with metabolic pathway regulation and cell signaling [10–13].

In carbohydrate transport, the first step in this cascade involves the phosphorylation of the substrate HPr by enzyme I ($EI^{sugar}$). The binding of HPr has been isolated to the N-terminal domain of $EI^{sugar}$ ($EIN^{sugar}$), while its C-terminal domain is important for phosphorylation, dimerization and phosphoenolpyruvate binding [14–17]. Multiple mechanisms are involved in PTS regulation. For instance, transcriptional regulation can increase or decrease the concentration of the enzymes and substrates for phosphotransfer depending on the amount of metabolites in the growth medium [3].

In addition, phosphorylation of the substrate HPr at a different site (Ser46) by an alternative ATP-dependent phosphorylation can provide a feedback mechanism for $EI^{sugar}$ activity [18–21]. Phosphoryl transfer between different components in the pathway occurs through an inline associative mechanism [22]. This transfer process involves transient heterodimeric interactions between the proteins in the pathway [3].

Enzyme–substrate interactions are driven by stereospecific binding of the substrate to the active site of the enzyme. This process is influenced by collision events due to random translational diffusion of the two proteins and can result in the formation of a transient encounter complex that might lead to a final stable complex [23–25]. In certain systems, the encounter complex is followed by a transition state, typically located closer to the final binding site, characterized by a few specific interactions [26–28] from which the stable complex is formed. Long-range electrostatic interactions and desolvation have been shown to be important driving forces in forming encounter complexes. An ensemble of conformations is formed that is in dynamic equilibrium with a dominant specific complex. Because of the above-mentioned driving forces, these complexes tend to be restricted to specific surfaces of the proteins. The encounter complexes keep the substrate on the enzyme surface for a long enough time, thereby locking the proteins in both productive and non-productive complexes, effectively increasing the local substrate concentration. Both types of complexes are key elements to consider when determining the probability of forming the stereospecific complex and changes in their populations could favor or impede this interaction.

Due to the transient nature of encounter complexes, they are particularly difficult to study. Paramagnetic centers, however, can be used to enhance the detection of these complexes and have been used to study various systems including a protein–DNA complex [29–31], cytochromes [32–35], heme transporters [36], and $PTS^{sugar}$ [37]. Tang *et al.* [37] identified encounter complexes between $EIN^{sugar}$ and HPr and isolated these complexes to specific surfaces on $EIN^{sugar}$. They also showed that these encounter complexes depend on electrostatic interactions between the two proteins [38]. In the case of $EI^{sugar}$ and HPr, this was illustrated by measuring the equilibrium dissociation constant between surface-charge swapped mutants of the two proteins and their native counterpart in conjunction with PRE probing of the corresponding population of the encounter complexes. It was shown that carefully engineered mutants can indeed control the equilibrium binding affinity [39].

In *E. coli*, there is a paralogous PTS for the regulation of nitrogen metabolism and a number of other cytosolic processes [40]. Its components closely parallel the sugar PTS with the caveat that the nitrogen PTS is instead a three-step cascade, owing to its simplified single domain EII [41]. The first phosphotransfer step in the cascade requires the interaction between the N-terminus of enzyme I ($EIN^{Ntr}$), and its substrate, NPr. Since the first step in these two PTSs involves homologous protein components and chemical processes, we hypothesized that HPr, the NPr paralog from $PTS^{sugar}$ with a similar fold but different surface profile, might influence the formation of the NPr:$EIN^{Ntr}$ phosphotransferase complex, hence coupling the nitrogen regulation pathway to carbohydrate transport.

We investigated the transient interaction between $EIN^{Ntr}$ (residues 170–424) and NPr by measuring the PRE of $EIN^{Ntr}$ resonances caused by the presence of nitroxide spin labels on NPr. Using three NPr mutants that have been covalently modified to incorporate a paramagnetic group, we observed large PRE values for residues in the stereospecific binding surface of NPr on $EIN^{Ntr}$, and at the same time identified encounter complexes in proximity to the specific binding site. We previously showed that HPr does not form a specific complex with $EIN^{Ntr}$ [42]. To test for a potential weak cross-pathway interaction involving EI, we measured PRE on $EIN^{Ntr}$ in the presence of a paramagnetic version of HPr, a substrate of $EIN^{sugar}$. Despite the absence of stereospecific interaction, we observed transient interactions between the two proteins. Furthermore, in direct competition experiments between NPr and HPr, we found that the HPr–$EIN^{Ntr}$ encounter complexes could block those of NPr and $EIN^{Ntr}$. More importantly, the population of NPr in the specific binding site was increased as shown by the consistently decreased resonance intensity due to the presence of the paramagnetic group. This unexpected finding might suggest a novel mechanism whereby competitive encounter complexes could funnel ligands like NPr toward their specific binding site. Competitive encounter complexes could prove to be a general mechanism for cross-regulation of parallel transport pathways without directly inhibiting specific binding of enzymes and substrates.

## Results

The first enzymatic step in the paralogous carbohydrate and nitrogen phosphotransferase systems in bacteria is composed of very similar components, the $EI^{sugar}$ and $EI^{Ntr}$ enzymes and their substrates HPr and NPr, respectively. The structure of the complex between the N-terminal domain, $EIN^{Ntr}$ and NPr [42] is shown in Fig. 1a and illustrates the intricate short-range atomic interactions that define their specificity. The structure of the complementary complex between $EIN^{sugar}$ and HPr has also been determined [43]. Strikingly, comparing the structure of the individual components of these complexes reveals their high

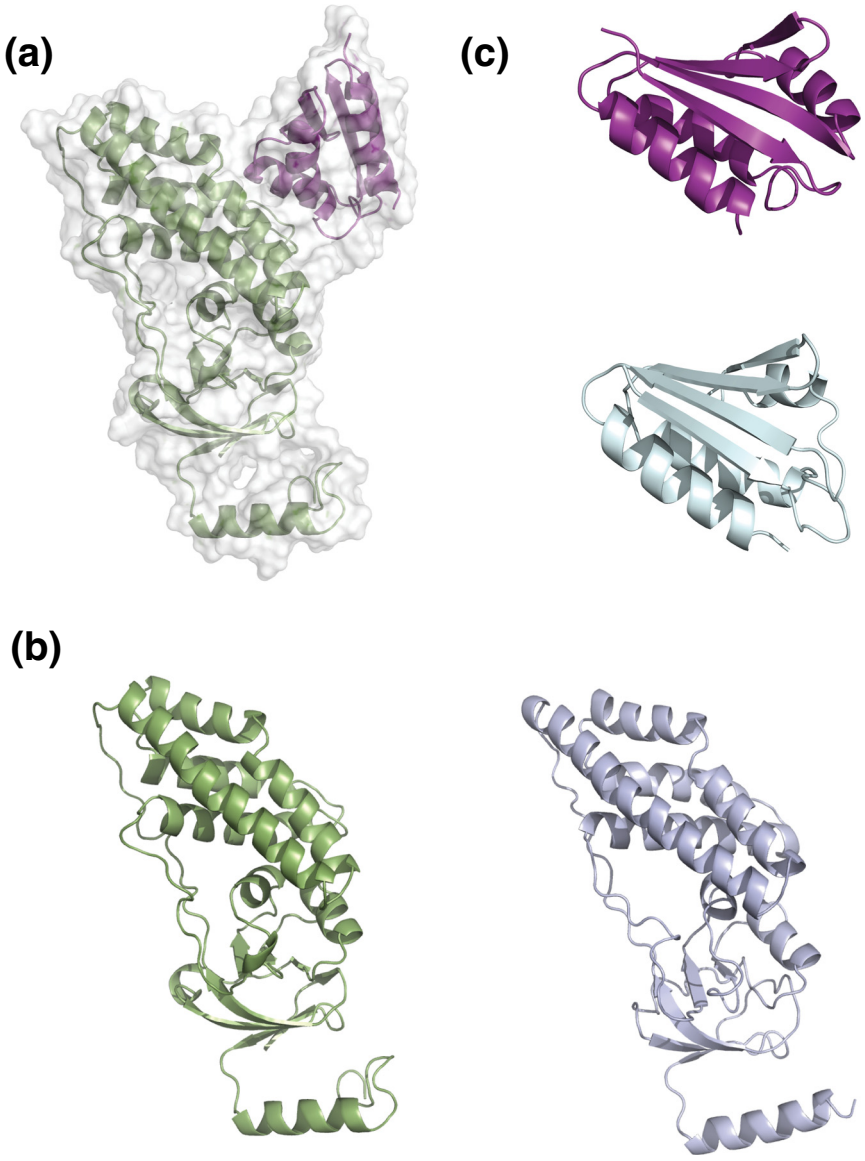


**Fig. 1.** Structural comparison of EIN and its substrate. Structure of the complex between $EIN^{Ntr}$ (green) and NPr (purple) is shown in panel a as ribbon and space-filled model (PDB ID: 5T1O [42]). (b) $EIN^{Ntr}$ (PDB: 5T1O) is shown in green, while $EIN^{sugar}$ (PDB: 3EZA [43]) is shown in light purple. The two enzymes have almost identical fold with pairwise Cα RMSD of 2.6 Å. (c) Their substrates NPr (PDB: 5T1O) shown in purple, and HPr (PDB: 3EZA) in light blue, are composed of similar tertiary fold with Cα RMSD of 2.4 Å. The molecular representations in all figures are generated using the program PyMol.

degree of similarity. The $EIN^{Ntr}$ (PDB: 5T1O) and $EIN^{sugar}$ (PDB: 3EZA) domains show a closely related three-dimensional fold with a pairwise RMSD of the Cα atoms of 2.6 Å (Fig. 1b). In addition, the backbone structures of their substrates NPr (PDB: 5T1O) and HPr (PDB ID: 3EZA) are also very similar with an RMSD of their Cα atoms of 2.4 Å (Fig. 1c).

Since the structures of these enzyme complexes are quite similar, it is reasonable to expect that their kinetics of interaction would also be comparable. Inspired by the extensive NMR work of Tang and colleagues [37] to visualize the transient interaction between $EIN^{sugar}$ and HPr, we set out to test if transient encounter complexes are also observable between $EIN^{Ntr}$ and NPr. We tagged an NPr mutant (T6C) with MTSL, a nitroxide spin label that induces enhanced $T_2$ relaxation in a distance-dependent manner [44]. In complexes that do not sample minor conformations or transient interactions, this distance dependence can be used to accurately predict the expected PRE induced by the paramagnetic tag by using the structure of the stable stereospecific complex. Instead, upon formation of the $^{2}H\text{-}NPr^{T6C\text{-}MTSL}$:$^{2}H/^{15}N\text{-}EIN^{Ntr\text{-}H356Q}$ complex, we found that the observed PREs did not match those

expected for the specific complex alone (Fig. 2a, Suppl. Fig. S1a), nor did they match any alternative single complex conformation. This indicated that there could be minor complexes or transient interactions occurring between NPr and $EIN^{Ntr}$, as was previously observed for the paralogous HPr:$EIN^{sugar}$ complex. To further investigate these interactions, PREs were measured for two more mutants of NPr, E45C and E74C. Their measured and expected PRE values for a single stereospecific complex are shown in Fig. 2b and c, respectively (see also Suppl. Fig. S1b and c, Suppl. Table 1). Similar to the T6C mutant, discrepancies between the observed and expected PREs confirmed the presence of encounter complexes. Residues with PRE discrepancies of more than 8 $s^{-1}$ are mapped onto the surface of $EIN^{Ntr}$ (Fig. 2). There are clear overlaps of the encounter complex surfaces on $EIN^{Ntr}$ derived from the data of the three NPr mutants. In all, 13 residues were categorized as "non-specific" NPr binders in all three MTSL-tagged mutants (those residues with $>8$ $s^{-1}$ discrepancy between the observed and calculated PRE, and a calculated PRE value of $<20$ $s^{-1}$). Although three residues are surface exposed (L191, E195, and the active-site H356Q mutation), the majority are inward-facing hydrophobic core residues located in and around a negatively charged cleft between the α- and the α/β-domains of $EIN^{Ntr}$ (Suppl. Fig. S2). Although Tang *et al.* [37] found that the encounter complexes for the HPr:$EIN^{sugar}$ interaction also occurred in a negatively charged region, they were predominantly located on the α-domain adjacent to the HPr binding site. Since it was previously shown that non-specific electrostatic interactions can contribute to the observed encounter complexes in the HPr:$EIN^{sugar}$ interaction [38], we carried out all of our NMR experiments in the presence

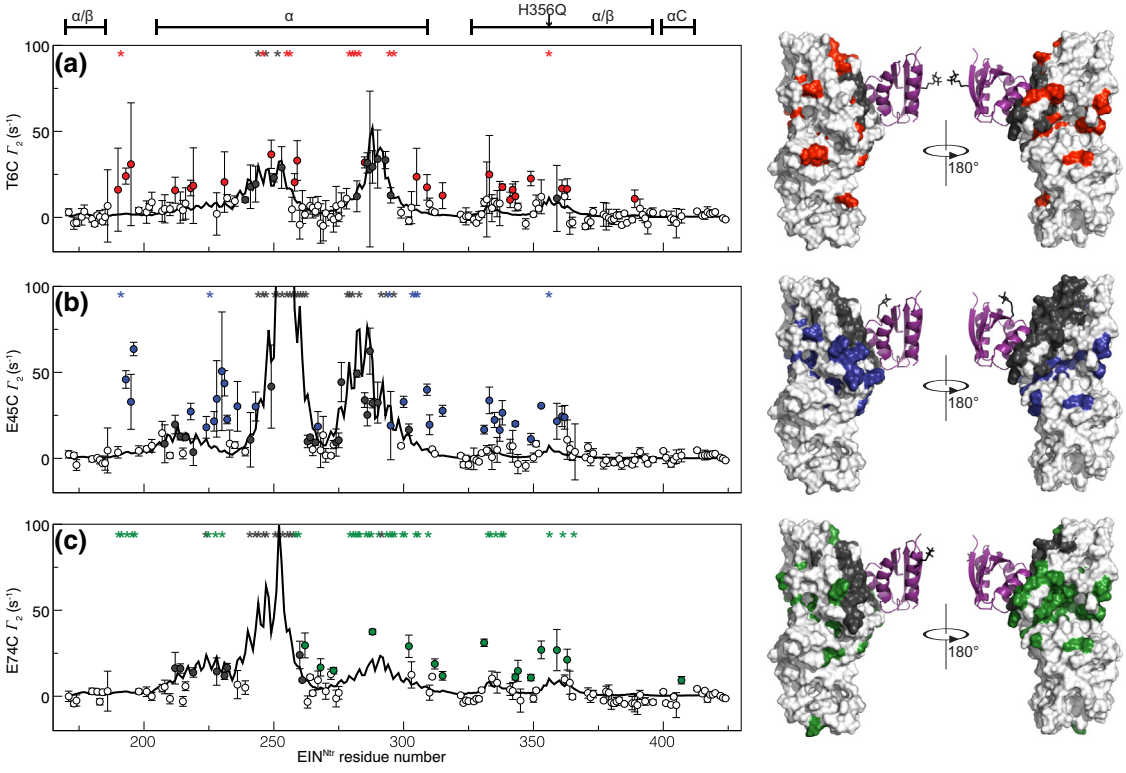


**Fig. 2.** Observed and calculated PREs for the NPr:$EIN^{Ntr}$ complex. The observed (circles) and back-calculated (black lines) intermolecular PREs for the NPr:$EIN^{Ntr}$ complex are shown for each of the three NPr mutants—T6C (a), E45C (b), and E74C (c). PREs were induced using a covalently attached MTSL spin label at each of the three positions. Stars represent residues whose peaks are broadened beyond detection in the paramagnetic samples. The $EIN^{Ntr}$ residues whose PRE discrepancies (between observed and calculated values) of more than 8 $s^{-1}$ (or are completely broadened out) and a calculated PRE value of $<20$ $s^{-1}$, are drawn in colored circles (or stars) and designated as "non-specific" binders. "Specific" residues are remaining residues with both observed and calculated PRE values of $>8$ $s^{-1}$ and are drawn with dark gray circles or stars. The approximate locations of the α-, α/β-, and C-terminal helix (αC) domains of $EIN^{Ntr}$ are displayed for comparison, along with the position of the active site H356Q mutation (arrow). On the right, the NPr:$EIN^{Ntr\text{-}H356Q}$ structure is shown, with $EIN^{Ntr}$ and NPr in white surface and purple ribbon representation, respectively (PDB: 5T1O [61]). "Non-specific" $EIN^{Ntr}$ residues are highlighted on the surface in red, blue, and green colors for the T6C, E45C, and E74C mutant, respectively, while "specific" residues are highlighted in dark gray. Error bars for observed PRE values are calculated as the propagated standard error for a set of two $R_2$ measurements and are listed with the PRE values in Suppl. Table 1.

of 100 mM salt to reduce the chance of observing the non-productive population of our encounter complexes.

Since the structures of the enzyme and substrate for these two phosphotransferase systems are quite similar, and encounter complexes have previously been observed in the sugar PTS, it is not surprising that we could observe transient encounters in the nitrogen PTS. Previously, we have shown that there is no stable cross-interaction between the first phosphotransfer step in these two pathways [42]. That is, no interaction could be detected between HPr and $EIN^{Ntr}$ by surface plasmon resonance (for $His_6$-$EIN^{Ntr\text{-}WT}$) or size exclusion chromatography (for $EIN^{Ntr\text{-}H356Q}$) [42]. This is completely expected because HPr and $EIN^{Ntr}$ are both positively charged in their respective binding sites, preventing cross-reaction between the pathways (similarly, NPr and $EIN^{sugar}$ are both negatively charged in the same regions; see Ref. [42], for a detailed comparison of the two complexes). Encounter complexes follow different kinetics, relying more on long-range interaction, compared to the stereospecific complex. In addition, the substrates and the enzymes in these two pathways have very similar geometry. Finally, both HPr and NPr form encounter complexes in negatively charged regions of $EIN^{sugar}$ and $EIN^{Ntr}$, respectively. Based on the above observations, it is reasonable to expect that cross-interaction of the encounter complexes for these two systems might be possible. Therefore, we tested if encounter interactions could be observed between HPr and $EIN^{Ntr}$. We measured PREs for $^{2}H/^{15}N$-$EIN^{Ntr\text{-}H356Q}$ in complex with $^{2}H$-$HPr^{E5C\text{-}MTSL}$ as a ratio between peak heights in an HSQC-TROSY of $EIN^{Ntr\text{-}H356Q}$ in the presence and absence of HPr (Fig. 3a, Suppl. Table 2). For comparison, we show the intensity ratios due to PRE for the homologous $NPr^{T6C\text{-}MTSL}$:$EIN^{Ntr\text{-}H356Q}$ complex (Fig. 3b). Since HPr does not interact specifically with $EIN^{Ntr}$, deviations from an average ratio indicate the presence of non-specific encounter complexes between the two proteins. Residues with an intensity ratio more than three standard deviations lower than the mean (high PRE) were identified as potential sites of encounter complexes and are highlighted in yellow and purple for $HPr^{E5C\text{-}MTSL}$ and $NPr^{T6C\text{-}MTSL}$, respectively (Fig. 3). In contrast to their specific interaction, the encounter complexes between these two enzymes appear to indicate that some cross-regulation might be occurring between the two phosphotransfer systems.

To assess both the relative strength of the HPr:$EIN^{Ntr}$ transient interactions relative to those found in NPr:$EIN^{Ntr}$ and the influence on the stereospecific NPr:$EIN^{Ntr}$ interaction, we set up a competition PRE experiment using the resonance intensity ratio to report changes in relaxation rates. This approach allows for a lower signal to noise ratio associated with dilution of $EIN^{Ntr}$ during the titration. In order to observe changes in PRE in the NPr:$EIN^{Ntr}$ complex caused by the addition of HPr, we calculated the ratio of peak heights of the $^{2}H$-$NPr^{E45C\text{-}MTSL}$:$^{2}H/^{15}N$-$EIN^{Ntr\text{-}H356Q}$ complex, in the presence and absence of $^{2}H$-$HPr^{WT}$. The observed changes in the peak height ratio upon addition of HPr are shown in Fig. 4a. With the addition of equimolar HPr to NPr (at a slight excess of 1.2× the concentration of $EIN^{Ntr}$), a notable decrease in $EIN^{Ntr}$ peak height was observed for residues close to the NPr:$EIN^{Ntr}$ specific complex interface with some resonances disappearing completely, accompanied by an increase in peak height in other areas (Fig. 4a, Suppl. Table 3). Consistent changes in the peak heights were observed upon further addition of HPr up to a ratio of 10:1, thus confirming these observations. As a control we carried out the same experiment substituting HPr with human ubiquitin [45]. No significant changes in peak heights were observed (Suppl. Fig. 3), indicating that the observed competition to NPr:$EIN^{Ntr}$ encounter complexes was specific to HPr.

Residues that increase in intensity with the addition of HPr represent a population with reduced paramagnetic effect and therefore less interaction with NPr. This could be due to the occupation of these sites by HPr. These residues fall in regions of $EIN^{Ntr}$ where non-specific complexes tend to be found (highlighted in gray, Fig. 4a). Conversely, those that decrease in intensity are experiencing increased PRE. This signifies increased lifetime at that site and, if it is within the stereospecific binding site, might be a result of increased stereospecific binding affinity of the NPr:$EIN^{Ntr}$ complex. Residues that undergo a large change (>3 SD from the mean change for non-binding residues, see Materials and Methods) at the 10:1 HPr:NPr ratio are plotted in Fig. 4b. Residues with decreased intensity (apparent higher affinity or longer lifetime) are found in the α-domain of $EIN^{Ntr}$ and close to the tagged residue E45C of NPr, while residues with increased intensity (apparent weaker affinity or shorter lifetime) are mostly in the α/β domain. Both sets of residues are mostly surface exposed and hydrophobic, with some charged or polar residues in each group. To quantify the population of residues experiencing different PRE changes relative to their location to the specific NPr:$EIN^{Ntr}$ binding site, we calculated the distribution of the distances to the $C^{\delta}$ atom of NPr residue E45 for the 10% of $EIN^{Ntr}$ residues with the largest decreased or increased peak height upon the addition of 10:1 HPr:NPr (17 residues in each group), with histograms shown in Fig. 4c and d, respectively. There is a maximum of distribution of number of residues with decreased intensity around 20–25 Å and one for those with increased intensity at around 35–40 Å.

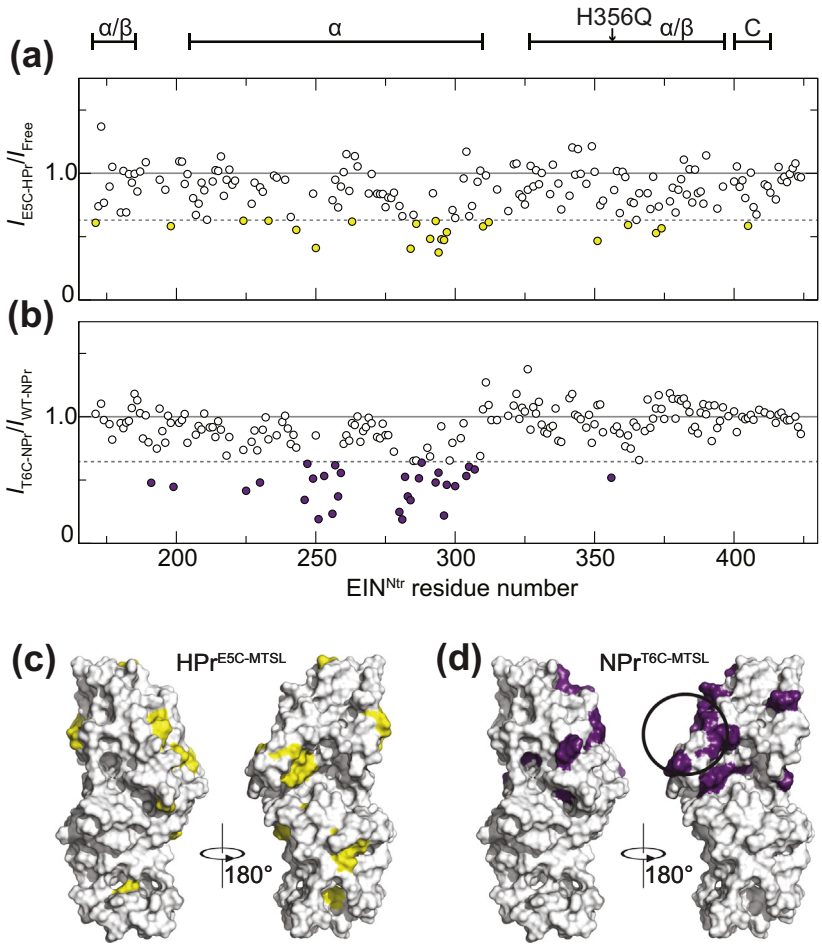


**Fig. 3.** Encounter complexes are observed between EIN$^{Ntr}$ and HPr. (a) Observed PRE ratios (circles) calculated using the EIN$^{Ntr\text{-}H356Q}$ resonance peak heights in the presence and absence of MTSL-tagged HPr$^{E5C}$. (b) Observed PRE ratios (circles) calculated for EIN$^{Ntr\text{-}H356Q}$ in the presence of NPr$^{T6C\text{-}MTSL}$ (paramagnetic) or NPr$^{WT}$ (diamagnetic). Results including errors (calculated from the spectral noise) are summarized in Suppl. Table 2. A ratio of 1, shown as a gray line, indicates no observed PRE. The dashed gray line indicates 3 SD below the mean PRE ratio for non-binding residues (see Materials and Methods). Significant PREs (below the dashed line) are shown in panels a and b, using yellow and purple circles, respectively. Significant PREs are also displayed on the surface of EIN$^{Ntr}$ induced by the presence of HPr$^{E5C\text{-}MTSL}$ in yellow (c) and NPr$^{T6C\text{-}MTSL}$ in purple (d). The stereospecific binding site of NPr on EIN$^{Ntr\text{-}H356Q}$ is circled in panel d.

## Discussion

The observation of encounter complexes between EIN$^{Ntr}$ and NPr, as also seen between EIN$^{sugar}$ and HPr, EII$^{mannose}$ and HPr, and EII$^{mannitol}$ and HPr, confirms the transient nature of interactions between this family of enzymes and their substrates [37]. Each enzyme–substrate pair establishes encounter interactions in a distinct manner. EIN$^{sugar}$ and HPr encounters were shown to occur on charged areas on the surface of the enzyme, suggesting interactions driven by electrostatics. The encounters involving charged interactions could be modulated by the addition of salt [38]. In contrast, the encounters between EIN$^{Ntr}$ and NPr seem to involve residues on EIN$^{Ntr}$ that although they occur in negatively charged regions of the protein, are much more hydrophobic in nature than those observed for EIN$^{sugar}$ (Suppl. Fig. 2, [37]). Because of the different nature of molecular interactions that drive the encounter formation in these two enzymes, it was surprising to observe cross-pathway encounter formation between EIN$^{Ntr}$ and HPr. On the other hand, perhaps this cross-interaction should have been expected, since the three-dimensional folds of both the enzymes and the substrates in these two paralogous PTS are almost identical. Thus, surface or shape complementarity between any substrate to any EI always exists, potentially promoting interaction between them. That being said, the presence of different surface compositions between the two enzymes could differentiate the observed encounter

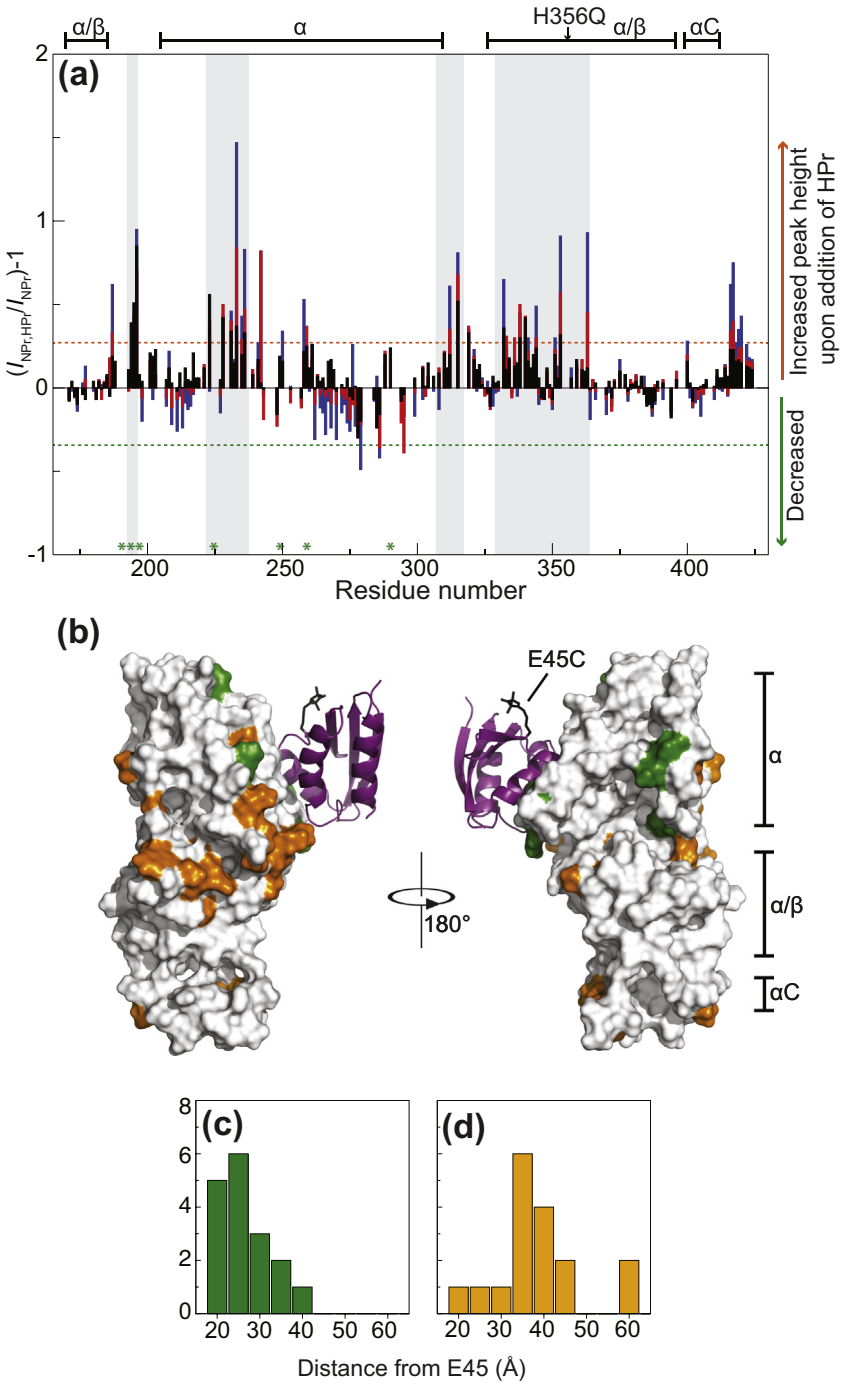


**Fig. 4.** Competitive encounter complexes between HPr and $EIN^{Ntr}$ increase stereospecific binding affinity of NPr:$EIN^{Ntr}$. (a) Changes in $EIN^{Ntr}$ resonance intensity for the $NPr^{E45C\text{-}MTSL}$:$EIN^{Ntr}$ complex as a function of HPr addition. Changes shown are at a 1:1, 5:1, and 10:1 molar ratio of HPr:NPr in black, red, and blue, respectively. Regions with large discrepancies between observed and calculated PRE values for the E45C $EIN^{Ntr}$ mutant are highlighted in gray (Fig. 2b). These regions correlate to areas with an increased peak height upon the addition of HPr. The α-, α/β-, and αC domains of $EIN^{Ntr}$ are shown at the top of the panel. The dotted lines are cutoffs for considering a residue as having a large decreased (green) or increased (orange) resonance intensity upon addition of 10-fold HPr relative to NPr (>3 SD from the mean PRE ratio for non-binding residues). A full list of results with errors can be found in Suppl. Table 3. (b) Residues with large (>3 SD from the mean) decreased (green) or increased (orange) resonance intensity upon the addition of 10-fold HPr relative to NPr, shown on the surface of $EIN^{Ntr}$ (PDB: 5T1O [42]). NPr is shown in purple ribbon representation, with residue E45 shown in black sticks. The α, α/β, and αC domains are indicated. Histograms of the distance between E45 $C^{\delta}$ and the backbone amide $H^{N}$ for the 10% of residues with the most decreased intensity (including broadened residues) upon the addition of HPr in panel b are shown in panel c, while those 10% with the most increased intensity are in panel d.

imprint of NPr on the surface of $EIN^{Ntr}$ from that of HPr. What is more intriguing is the overlap between the encounter surfaces because this allows for potential competition between the two substrates in forming the encounter surface on $EIN^{Ntr}$, which was observed.

It is important to note that most encounter complexes are non-productive, that is, they generally do not transform into a stable specific complex [24,46,47]. These non-productive encounter sites in general are distant to the specific binding site of the complex and enlarging or reducing these areas by introducing mutations does not seem to affect their final association rate [48]. Mutations that increase the rate of successful associations are instead correlated to an increase in the area of the encounter region near the transition state [48]. Furthermore, the study of the barnase–barstar system identified a narrower and more specific transition state than the encounter complexes [26,49]. This could be interpreted as an

energetic funnel with a broader encounter complex population that feeds into a narrower transition state leading to the final complex [48]. This notion of driving encounter population toward the stereospecific complex site is also consistent with the discovery of multiple classes of encounter complexes, based on the PRE profile as a function of the relative concentration between HPr and $EIN^{sugar}$ [17,50]. Our data seem to add to the above line of observations. Forcing the encounter complexes of NPr, by competition with HPr, to occupy only sites close to the stereospecific site on $EIN^{Ntr}$ increases the chance for productive association corresponding to the observed decrease in resonance peak heights (Fig. 4). The 10% of residues in $EIN^{Ntr}$ with the most increased probability of association (T190, M194, V197, R211, T213, R224, L249, F259, V262, S266, A268, W270, V275, K278, F279, L286, and Y290) with NPr in the presence of HPr are located closer to the NPr binding site with the maximum population located largely in the α-helical domain around 25 Å away (measured to NPr residue E45 in the NPr:$EIN^{Ntr}$ complex structure), while residues with decreased probability of association (Q187, Q196, A231, G233, Q235, K236, F242, L258, A312, G315, A332, L338, V344, A353, A363, S416, and R417) were located further away, generally in the α/β-domain, with the maximum distribution around 35 Å.

One potential factor that could lead to the above competition of encounter complexes is the effect of crowding. This is unlikely, considering that the concentrations of the proteins used in the experiments are lower than that used in typical crowding experiments, which is a minimum of a few percent of the total volume of the sample. In addition, the crowding effect has previously been shown not to increase the final association rate due to two opposing factors. Slow diffusion in a crowded environment reduces the number of molecular collisions that lead to encounter complex formation, while the excluded volume effect increases the effective non-specific attraction between the proteins [51]. We nevertheless tested the possibility of non-specific crowding by using ubiquitin in place of HPr in the competition experiment and could not see any effect on the formation of $EIN^{Ntr}$:NPr encounter complexes (Suppl. Fig. 2).

Partitions of enzymes and substrates into different cellular compartments contribute to their relative concentrations. Due to their functions, the enzymes I for sugar transport and nitrogen regulation are proximal to each other in the cell. Therefore, their total cellular concentrations are directly relevant to compare for potentially forming cross-encounter complexes. HPr and its specific partner $EI^{sugar}$ are some of the most highly abundant proteins in the *E. coli* cytoplasm, with HPr concentrations ~50 times higher than that of $EI^{Ntr}$ and more than 150 times higher than NPr (integrated whole-genome data taken from the PaxDb protein abundance database, see Materials and Methods). As such, it is conceivable that these transient interactions observed between HPr and $EIN^{Ntr}$ could be sampled often enough to act in a competitive manner with NPr encounter binding. Our findings suggest that the substrate (HPr) of enzyme $EIN^{sugar}$, which is present in a much higher concentration than the other (NPr) can influence a paralogous enzyme ($EIN^{Ntr}$) function. Rather than directly inhibiting access to the specific binding site of NPr in $EIN^{Ntr}$, HPr effectively funnels NPr to encounter sites close to the final stereospecific site by occupying "unproductive" encounter sites thus increasing NPr's specific binding affinity. Perhaps this might be a mechanism of cross-regulation for systems with similar structures that utilize transient molecular interactions for protein-substrate complexes.

## Materials and Methods

### Cloning and purification of proteins

*E. coli* $HPr^{WT}$, $NPr^{WT}$ (residues 1–85), $EIN^{Ntr\text{-}H356Q}$ (residues 170-424 of $EI^{Ntr}$), and *Homo sapiens* $Ub^{WT}$ were expressed and purified as previously described [42,45,52,53]. $HPr^{E5C}$, $NPr^{T6C}$, $NPr^{E45C}$, and $NPr^{E74C}$ were produced from the corresponding wild-type using a QuikChange mutagenesis kit (Agilent). $^{2}H_2O$ and $^{15}N$-ammonium chloride were used with M9 minimal media to produce $^{2}H$- and $^{2}H/^{15}N$-labeled proteins from $NiCo_{21}$(DE3) *E. coli* cells (pETDuet-1 plasmids). All constructs were expressed as soluble proteins and were purified using a MonoQ column [10 mM Tris, 0.5 mM EDTA, 2 mM EDTA (pH 7.5), gradient: 0–500 mM NaCl], followed by either a Sephadex 75 column ($HPr^{E5C}$) or a Superose 12 column (NPr mutants) run with the following buffer: 10 mM Tris (pH 7.5), 0.5 mM EDTA, and 2 mM DTT. Proper folding of the mutants in comparison to the wild-type proteins was confirmed by 1D proton NMR spectroscopy.

### Attachment of MTSL tag to HPr and NPr

DTT (2 mM) was added to $^{2}H\text{-}HPr^{E5C}$, $^{2}H\text{-}NPr^{T6C}$, $^{2}H\text{-}NPr^{E45C}$, or $^{2}H\text{-}NPr^{E74C}$ [in 10 mM Tris, 100 mM NaCl, 0.5 mM EDTA (pH 7.5), ~2.5 mg protein in 500 µL buffer] and incubated at room temperature for 1 h to reduce any disulfide bonds present in the samples. Full reduction was confirmed using a 1D proton spectrum. DTT was removed using a PD-10 column [GE Healthcare, PD-10 buffer: 10 mM Tris, 100 mM NaCl, 0.5 mM EDTA (pH 7.5)], whereupon the protein was dripped directly into a solution of *S*-(1-oxyl-2,2,5,5-tetramethyl-2,5-dihydro-1*H*-pyrrol-3-yl)methylmethanesulfonothioate (MTSL; Toronto

Research Chemicals) dissolved in DMSO (10 mM stock solution, 10:1 excess MTSL/protein during reaction, protein ~70 μM in a 3.5 mL volume of PD-10 buffer). Following 16 h of incubation at room temperature, excess DMSO and unreacted MTSL tag were removed using Amicon Ultra-4 centrifugal filters (3 kDa MWCO). Successful MTSL tag attachment was confirmed by electrospray ionization time-of-flight liquid chromatography–mass spectrometry and by the observation of relaxation in a 1D proton NMR spectrum.

### Solution NMR experiments

$^{2}$H-HPr$^{E5C\text{-}MTSL}$, $^{2}$H-NPr$^{T6C\text{-}MTSL}$, $^{2}$H-NPr$^{E45C\text{-}MTSL}$, $^{2}$H-NPr$^{E74C\text{-}MTSL}$, or $^{2}$H-NPr$^{WT}$ were complexed with $^{2}$H/$^{15}$N-EIN$^{H356Q}$ in a 1.2:1 ratio, which resulted in a final EIN$^{H356Q}$ concentration of 150 μM [in 10 mM Tris, 100 mM NaCl, 0.5 mM EDTA (pH 7.5), 8% $D_2O$]. In competition experiments, $^{2}$H-HPr$^{WT}$ or $^{2}$H-Ub$^{WT}$ were added to the $^{2}$H/$^{15}$N-EIN$^{H356Q}$:$^{2}$H-NPr$^{E45C\text{-}MTSL}$ complex in a 1:1, 5:1, and 10:1 ratio of HPr/NPr or Ub/NPr. NMR data were acquired at 300 K on a Bruker Avance 800 MHz spectrometer, equipped with a cryogenic probe. Spectra were processed using NMRPipe [54] and analyzed using CCPN Analysis 2.4.2 [55]. EIN$^{Ntr\text{-}H356Q}$ backbone chemical shifts, both free and in complex with NPr$^{WT}$, were previously assigned (BMRB: 30159) [42] and were used as the basis for assignment of the mutant spectra. PREs were measured as the difference between spectra measured in diamagnetic and paramagnetic conditions by one of two methods. For the diamagnetic NPr$^{WT}$ and the paramagnetic MTSL-tagged NPr mutants (T6C, E45C, and E74C) in complex with EIN$^{Ntr\text{-}H356Q}$, amide proton $T_2$ values were calculated by fitting an exponential decay curve to peak heights measured in $T_2$ experiments with delays of 0.04, 1, 2, 3, 4, 6, 12, 24, and 36 ms. PRE values were calculated using the following equation: $\Gamma_2 = R_{2,para} - R_{2,dia}$ [30]. For these experiments, an offset of 5.28 was subtracted from the PRE values. Error bars are ±1 standard error for two sets of paramagnetic and diamagnetic $R_2$ measurements ($SD_{R2,para}$ + $SD_{R2,dia}$). For the remaining experiments, PRE was analyzed by directly comparing the ratio of peak heights in TROSY–HSQC spectra of diamagnetic and paramagnetic samples. Weak and/or overlapped peaks were removed from the analysis. Weak peaks were defined as less than five times the noise in a peak-free area as calculated using the RMSD function of Sparky (T. D. Goddard and D. G. Kneller, University of California, San Francisco). To compare PRE ratios of samples at different concentrations (for example in the competition experiments), peak height ratios were normalized by dividing by the median peak height ratio in areas with no changes between experiments. For HPr$^{E5C\text{-}MTSL}$ and NPr$^{T6C\text{-}MTSL}$ encounter complex experiments, error bars were calculated from the propagated experimental noise, measured using the RMSD function in Sparky. For HPr/NPr$^{E45C\text{-}MTSL}$ competition experiments, error bars were calculated from the propagated standard error of two sets of experiments. All PRE values and error bars are summarized in Suppl. Tables 1–3.

### Calculation of expected PRE values for the specific EIN$^{Ntr}$:NPr complex

PREs were back-calculated for each of the three MTSL-tagged NPr mutants (T6C, E45C, and E74C) in complex with EIN$^{Ntr}$ using the published structure of the specific NPr:EIN$^{Ntr}$ complex (PDB ID: 5T1O) [42]. PRE rates were calculated using the correlation function of the calcPRE helper program in Xplor-NIH 2.49.1 [56,57]. One copy of MTSL was used at each position, and the position of the tag was optimized using simulated annealing in torsion angle space to fit the PRE data, as described previously [29]. The optimization requires an estimate of the PRE correlation time ($\tau_c$), which is defined as $\tau_c^{-1} = \tau_r^{-1} + \tau_s^{-1}$, where $\tau_r$ is the rotational correlation time for the protein complex and $\tau_s$ is the electron relaxation time for MTSL, of which the latter is assumed to be negligible [44]. The protein rotational correlation time was assumed to be approximately the same as for the homologous HPr:EIN$^{sugar}$ complex ($\tau_r$ = 14.2 ns) [37].

### Determination of specific and non-specific binding residues

EIN$^{Ntr}$ residues were categorized as specific or non-specific binding according to the following rules (adapted from Ref. [50]): Non-specific residues (those in encounter complexes) must have a calculated PRE value of less than 20 $s^{-1}$, and a difference between observed and calculated PRE of more than 8 $s^{-1}$ (or are broadened completely in the paramagnetic spectra). Specific residues must not already be categorized as non-specific and must have an observed and calculated PRE value of more than 8 $s^{-1}$ (or are broadened completely in the paramagnetic spectra). The cutoff of 8 $s^{-1}$ was chosen as it is more than two standard deviations for all three mutants, where the standard deviation was calculated as the difference between the observed and calculated PRE values for those residues with PRE values $< 20$ $s^{-1}$ (PRE values of $> 20$ $s^{-1}$ can be inaccurate), as described by Fawzi *et al.* [50] in 2010. The standard deviation values for the three mutants were 3.9, 3.4, and 3.4 $s^{-1}$ for the T6C, E45C, and E74C mutants, respectively.

### Determination of cutoff values for significance for HPr encounter complex experiments

Cutoff values were determined using the mean and standard deviation for residues with PRE ratios that corresponded to PRE values of $<20\ s^{-1}$ (i.e., any value above 0.78 for $I_{E5C\text{-}HPr}/I_{Free}$ and $I_{T6C\text{-}NPr}/I_{WT\text{-}NPr}$, or less than ±0.22 from zero for $(I_{NPr,HPr}/I_{NPr}) - 1$). The conversion of a PRE value of 20 $s^{-1}$ to a PRE ratio of 0.78 was done using the average $NPr^{T6C\text{-}MTSL}$-induced $EIN^{Ntr}$ PRE ratio for residues with PRE values between 15 and 25 $s^{-1}$. Cutoff values for significance were determined to be >3 SD from the mean (below 0.633 for $I_{E5C\text{-}HPr}/I_{Free}$, below 0.644 for $I_{T6C\text{-}NPr}/I_{WT\text{-}NPr}$, and above and below 0.271 and −0.315 for $(I_{NPr,HPr}/I_{NPr}) - 1$).

### Relative abundance of proteins in *E. coli*

The relative abundance of HPr, NPr, $EI^{Ntr}$, and $EI^{sugar}$ was estimated using the webserver PaxDb version 4 (www.pax-db.org), a standardized database of protein abundance averages (as of May 2nd, 2017), using the "integrated" metadata set for *E. coli* [58], Relative abundances (in ppm) are 27.1 ($EI^{Ntr}$), 9.46 (NPr), 1103 ($EI^{sugar}$), and 1441 (HPr), giving percentiles (where *percentile* = 1 − (rank/total number of proteins)) of 64% ($EI^{Ntr}$), 54% (NPr), 96% ($EI^{sugar}$), and 97% (HPr).

### Generation of figures

Figures were generated using PyMol [59], Grace, NMRDraw [54], and UCSF Chimera [60].

## Acknowledgments

We thank Duck-Yeon Lee (National Heart, Lung, and Blood Institute) for assistance with liquid chromatography–mass spectrometry data. This work was supported by the Intramural Research Program of the National Heart, Lung, and Blood Institute and the Center for Information Technology of the National Institutes of Health.

## Appendix A. Supplementary data

Supplementary data to this article can be found online at https://doi.org/10.1016/j.jmb.2019.04.040.

*Received 26 February 2019;*
*Received in revised form 22 April 2019;*
*Available online 6 May 2019*

***Keywords:***
NMR;
paramagnetic relaxation enhancement (PRE);
encounter complex;
nitrogen phosphotransferase system ($PTS^{Ntr}$);
Enzyme I

Present address: S. Kale, National Library of Medicine, National Institutes of Health, Bethesda, MD 20892, USA.

†Contact: Building 50, Room 2316, NHLBI, NIH, Bethesda, MD 20892, USA.

***Abbreviations used:***
EI, enzyme I; HPr, phosphocarrier protein; EII, enzyme II; MTSL, *S*-(1-oxyl-2,2,5,5-tetramethyl-2,5-dihydro-1*H*-pyrrol-3-yl)methylmethanesulfonothioate.

## References

[1] W. Kundig, S. Ghosh, S. Roseman, Phosphate bound to histidine in a protein as an intermediate in a novel phospho-transferase system, Proc Natl Acad Sci U S A. 52 (1964) 1067–1074.
[2] M.H. Saier Jr., Evolution of transport proteins, Genet Eng (N Y). 23 (2001) 1–10.
[3] J. Deutscher, C. Francke, P.W. Postma, How phosphotransferase system-related protein phosphorylation regulates carbohydrate metabolism in bacteria, Microbiol Mol Biol Rev. 70 (2006) 939–1031.
[4] M.H. Saier, R.N. Hvorup, R.D. Barabote, Evolution of the bacterial phosphotransferase system: from carriers and enzymes to group translocators, Biochem Soc Trans. 33 (2005) 220–224.
[5] M.H. Saier Jr., J. Reizer, Proposed uniform nomenclature for the proteins and protein domains of the bacterial phosphoenolpyruvate: sugar phosphotransferase system, J Bacteriol. 174 (1992) 1433–1438.
[6] J.W. Lengeler, K. Jahreis, U.F. Wehmeier, Enzymes II of the phospho enol pyruvate-dependent phosphotransferase systems: their structure and function in carbohydrate transport, Biochim Biophys Acta. 1188 (1994) 1–28.
[7] P.W. Postma, J.W. Lengeler, G.R. Jacobson, Phosphoenolpyruvate:carbohydrate phosphotransferase systems of bacteria, Microbiol Rev. 57 (1993) 543–594.
[8] G.T. Robillard, J. Broos, Structure/function studies on the bacterial carbohydrate transporters, enzymes II, of the phosphoenolpyruvate-dependent phosphotransferase system, Biochim Biophys Acta. 1422 (1999) 73–104.
[9] C. Siebold, B. Erni, Intein-mediated cyclization of a soluble and a membrane protein in vivo: function and stability, Biophys Chem. 96 (2002) 163–171.
[10] Y.J. Seok, M. Sondej, P. Badawi, M.S. Lewis, M.C. Briggs, H. Jaffe, et al., High affinity binding and allosteric regulation of *Escherichia coli* glycogen phosphorylase by the histidine phosphocarrier protein, HPr, J Biol Chem. 272 (1997) 26511–26521.
[11] M. Sondej, A.B. Weinglass, A. Peterkofsky, H.R. Kaback, Binding of enzyme IIAGlc, a component of the phosphoenolpyruvate:sugar phosphotransferase system, to the *Escherichia coli* lactose permease, Biochemistry. 41 (2002) 5556–5565.

[12] R. Lux, K. Jahreis, K. Bettenbrock, J.S. Parkinson, J.W. Lengeler, Coupling the phosphotransferase system and the methyl-accepting chemotaxis protein-dependent chemotaxis signaling pathways of *Escherichia coli*, Proc Natl Acad Sci U S A. 92 (1995) 11583–11587.
[13] Y.H. Park, B.R. Lee, Y.J. Seok, A. Peterkofsky, In vitro reconstitution of catabolite repression in *Escherichia coli*, J Biol Chem. 281 (2006) 6448–6454.
[14] F. Chauvin, L. Brand, S. Roseman, Enzyme I: the first protein and potential regulator of the bacterial phosphoenolpyruvate: glycose phosphotransferase system, Res Microbiol. 147 (1996) 471–479.
[15] L.F. Garcia-Alles, K. Flukiger, J. Hewel, R. Gutknecht, C. Siebold, S. Schurch, et al., Mechanism-based inhibition of enzyme I of the *Escherichia coli* phosphotransferase system. Cysteine 502 is an essential residue, J Biol Chem. 277 (2002) 6934–6942.
[16] Y.J. Seok, B.R. Lee, C. Gazdar, I. Svenson, N. Yadla, A. Peterkofsky, Importance of the region around glycine-338 for the activity of enzyme I of the *Escherichia coli* phosphoenol-pyruvate:sugar phosphotransferase system, Biochemistry. 35 (1996) 236–242.
[17] G.M. Clore, V. Venditti, Structure, dynamics and biophysics of the cytoplasmic protein–protein complexes of the bacterial phosphoenolpyruvate: sugar phosphotransferase system, Trends Biochem Sci. 38 (2013) 515–530.
[18] G.F. Audette, R. Engelmann, W. Hengstenberg, J. Deutscher, K. Hayakawa, J.W. Quail, et al., The 1.9 A resolution structure of phospho-serine 46 HPr from *Enterococcus faecalis*, J Mol Biol. 303 (2000) 545–553.
[19] V. Monedero, S. Poncet, I. Mijakovic, S. Fieulaine, V. Dossonnet, I. Martin-Verstraete, et al., Mutations lowering the phosphatase activity of HPr kinase/phosphatase switch off carbon metabolism, EMBO J. 20 (2001) 3928–3937.
[20] J. Reizer, S.L. Sutrina, L.F. Wu, J. Deutscher, P. Reddy, M.H. Saier Jr., Functional interactions between proteins of the phosphoenolpyruvate:sugar phosphotransferase systems of *Bacillus subtilis* and *Escherichia coli*, J Biol Chem. 267 (1992) 9158–9169.
[21] M. Wittekind, J. Reizer, J. Deutscher, M.H. Saier, R.E. Klevit, Common structural changes accompany the functional inactivation of HPr by seryl phosphorylation or by serine to aspartate substitution, Biochemistry. 28 (1989) 9908–9912.
[22] G.S. Begley, D.E. Hansen, G.R. Jacobson, J.R. Knowles, Stereochemical course of the reactions catalyzed by the bacterial phosphoenolpyruvate:glucose phosphotransferase system, Biochemistry. 21 (1982) 5552–5556.
[23] A.R. Fersht, Structure and Mechanism in Protein Science, W. H. Freeman and Company, New York, 1999.
[24] G. Schreiber, Kinetic studies of protein–protein interactions, Curr Opin Struct Biol. 12 (2002) 41–47.
[25] J. Janin, The kinetics of protein–protein recognition, Proteins. 28 (1997) 153–161.
[26] M. Harel, M. Cohen, G. Schreiber, On the dynamic nature of the transition state for protein–protein association as determined by double-mutant cycle analysis and simulation, J Mol Biol. 371 (2007) 180–196.
[27] R. Alsallaq, H.X. Zhou, Energy landscape and transition state of protein–protein association, Biophys J. 92 (2007) 1486–1502.
[28] R. Alsallaq, H.X. Zhou, Prediction of protein–protein association rates from a transition-state theory, Structure. 15 (2007) 215–224.
[29] J. Iwahara, C.D. Schwieters, G.M. Clore, Ensemble approach for NMR structure refinement against (1)H paramagnetic relaxation enhancement data arising from a flexible paramagnetic group attached to a macromolecule, J Am Chem Soc. 126 (2004) 5879–5896.
[30] J. Iwahara, C.D. Schwieters, G.M. Clore, Characterization of nonspecific protein–DNA interactions by 1H paramagnetic relaxation enhancement, J Am Chem Soc. 126 (2004) 12800–12808.
[31] J. Iwahara, G.M. Clore, Detecting transient intermediates in macromolecular binding by paramagnetic NMR, Nature. 440 (2006) 1227–1230.
[32] A.N. Volkov, J.A. Worrall, E. Holtzmann, M. Ubbink, Solution structure and dynamics of the complex between cytochrome c and cytochrome *c* peroxidase determined by paramagnetic NMR, Proc Natl Acad Sci U S A. 103 (50) (2006), 18945.
[33] R. Hulsker, M.V. Baranova, G.S. Bullerjahn, M. Ubbink, Dynamics in the transient complex of plastocyanin–cytochrome f from *Prochlorothrix hollandica*, J Am Chem Soc. 130 (2008) 1985–1991.
[34] X. Xu, W. Reinle, F. Hannemann, P.V. Konarev, D.I. Svergun, R. Bernhardt, et al., Dynamics in a pure encounter complex of two proteins studied by solution scattering and paramagnetic NMR spectroscopy, J Am Chem Soc. 130 (2008) 6395–6403.
[35] S. Scanu, J.M. Foerster, G.M. Ullmann, M. Ubbink, Role of hydrophobic interactions in the encounter complex formation of the plastocyanin and cytochrome f complex revealed by paramagnetic NMR spectroscopy, J Am Chem Soc. 135 (2013) 7681–7692.
[36] V.A. Villareal, T. Spirig, S.A. Robson, M. Liu, B. Lei, R.T. Clubb, Transient weak protein–protein complexes transfer heme across the cell wall of *Staphylococcus aureus*, J Am Chem Soc. 133 (2011) 14176–14179.
[37] C. Tang, J. Iwahara, G.M. Clore, Visualization of transient encounter complexes in protein–protein association, Nature. 444 (2006) 383–386.
[38] J.Y. Suh, C. Tang, G.M. Clore, Role of electrostatic interactions in transient encounter complexes in protein–protein association investigated by paramagnetic relaxation enhancement, J Am Chem Soc. 129 (2007) 12954–12955.
[39] S.Y. An, E.H. Kim, J.Y. Suh, Facilitated protein association via engineered target search pathways visualized by paramagnetic NMR spectroscopy, Structure. 26 (2018) 887–893 e2.
[40] A. Peterkofsky, G. Wang, Y.J. Seok, Parallel PTS systems, Arch Biochem Biophys. 453 (2006) 101–107.
[41] Rabus R, Reizer J, Paulsen I, Saier MH, Jr. Enzyme I(Ntr) from *Escherichia coli*. A novel enzyme of the phosphoenolpyruvate-dependent phosphotransferase system exhibiting strict specificity for its phosphoryl acceptor, NPr. J Biol Chem. 1999;274: 26185-91.
[42] M. Strickland, A.M. Stanley, G. Wang, I. Botos, C.D. Schwieters, S.K. Buchanan, et al., Structure of the NPr:EIN(Ntr) complex: mechanism for specificity in paralogous phosphotransferase systems, Structure. 24 (2016) 2127–2137.
[43] D.S. Garrett, Y.J. Seok, A. Peterkofsky, A.M. Gronenborn, G.M. Clore, Solution structure of the 40,000 Mr phosphoryl transfer complex between the N-terminal domain of enzyme I and HPr, Nat Struct Biol. 6 (1999) 166–173.
[44] G.M. Clore, J. Iwahara, Theory, practice, and applications of paramagnetic relaxation enhancement for the characterization of transient low-population states of biological macromolecules and their complexes, Chem Rev. 109 (2009) 4108–4139.
[45] G.A. Lazar, J.R. Desjarlais, T.M. Handel, De novo design of the hydrophobic core of ubiquitin, Protein Sci. 6 (1997) 1167–1178.

[46] T. Selzer, G. Schreiber, New insights into the mechanism of protein–protein association, Proteins. 45 (2001) 190–198.
[47] C. Kiel, T. Selzer, Y. Shaul, G. Schreiber, C. Herrmann, Electrostatically optimized Ras-binding Ral guanine dissociation stimulator mutants increase the rate of association by stabilizing the encounter complex, Proc Natl Acad Sci U S A. 101 (2004) 9223–9228.
[48] M. Harel, A. Spaar, G. Schreiber, Fruitful and futile encounters along the association reaction between proteins, Biophys J. 96 (2009) 4237–4248.
[49] A. Spaar, C. Dammer, R.R. Gabdoulline, R.C. Wade, V. Helms, Diffusional encounter of barnase and barstar, Biophys J. 90 (2006) 1913–1924.
[50] N.L. Fawzi, M. Doucleff, J.Y. Suh, G.M. Clore, Mechanistic details of a protein–protein association pathway revealed by paramagnetic relaxation enhancement titration measurements, Proc Natl Acad Sci U S A. 107 (2010) 1379–1384.
[51] Y. Phillip, M. Harel, R. Khait, S. Qin, H.X. Zhou, G. Schreiber, Contrasting factors on the kinetic path to protein complex formation diminish the effects of crowding agents, Biophys J. 103 (2012) 1011–1019.
[52] X. Li, A. Peterkofsky, G. Wang, Solution structure of NPr, a bacterial signal-transducing protein that controls the phosphorylation state of the potassium transporter-regulating protein IIA Ntr, Amino Acids. 35 (2008) 531–539.
[53] P. Reddy, N. Fredd-Kuldell, E. Liberman, A. Peterkofsky, Overproduction and rapid purification of the phosphoenolpyruvate:sugar phosphotransferase system proteins enzyme I, HPr, and Protein IIIGlc of *Escherichia coli*, Protein Expr Purif. 2 (1991) 179–187.
[54] F. Delaglio, S. Grzesiek, G.W. Vuister, G. Zhu, J. Pfeifer, A. Bax, NMRPipe: a multidimensional spectral processing system based on UNIX pipes, J Biomol NMR. 6 (1995) 277–293.
[55] W.F. Vranken, W. Boucher, T.J. Stevens, R.H. Fogh, A. Pajon, M. Llinas, et al., The CCPN data model for NMR spectroscopy: development of a software pipeline, Proteins. 59 (2005) 687–696.
[56] C.D. Schwieters, J.J. Kuszewski, N. Tjandra, G.M. Clore, The Xplor-NIH NMR molecular structure determination package, J Magn Reson. 160 (2003) 65–73.
[57] C.D. Schwieters, J.J. Kuszewski, G.M. Clore, Using Xplor-NIH for NMR molecular structure determination, Prog Nucl Mag Res Sp. 48 (2006) 47–62.
[58] M. Wang, C.J. Herrmann, M. Simonovic, D. Szklarczyk, C. von Mering, Version 4.0 of PaxDb: Protein abundance data, integrated across model organisms, tissues, and cell-lines, Proteomics. 15 (2015) 3163–3168.
[59] PyMOL. The PyMOL Molecular Graphics System, Version 1.5.0.3 Schrödinger, LLC.; 2012.
[60] E.F. Pettersen, T.D. Goddard, C.C. Huang, G.S. Couch, D.M. Greenblatt, E.C. Meng, et al., UCSF Chimera—a visualization system for exploratory research and analysis, J Comput Chem. 25 (2004) 1605–1612.
[61] M. Strickland, A.M. Stanley, G. Wang, I. Botos, C.D. Schwieters, S.K. Buchanan, et al., Structure of the NPr:EINNtr complex: mechanism for specificity in paralogous phosphotransferase systems, Structure. 24 (2016) 2127–2137.